Research Paper

miR-128 participates in the pathogenesis of slow transit constipation by regulating the p38α/M-CSF inflammatory signaling pathway

Yuntian Hong[1,2,3,*], Weicheng Liu[1,2,3,4,5,*], Bo Liu[1,2,3,*], Xianghai Ren[1,2,3,4,5], Kongliang Sun[1,2,3], Xueqiao Yu[1,2,3,4,5], Quanjiao Chen[6], Qun Qian[1,2,3,4,5], Xiaoyu Xie[1,2,3,4,5], Congqing Jiang[1,2,3,4,5]

[1]Department of Colorectal and Anal Surgery, Zhongnan Hospital of Wuhan University, Wuhan 430071, China
[2]Clinical Center of Intestinal and Colorectal Diseases of Hubei Province, Wuhan 430071, China
[3]Hubei Key Laboratory of Intestinal and Colorectal Diseases (Zhongnan Hospital of Wuhan University), Wuhan 430071, China
[4]Colorectal and Anal Disease Research Center of Medical School (Zhongnan Hospital of Wuhan University), Wuhan 430071, China
[5]Quality Control Center of Colorectal and Anal Surgery of Health Commission of Hubei Province, Wuhan 430071, China
[6]CAS Key Laboratory of Special Pathogens and Biosafety, Wuhan Institute of Virology, Center for Biosafety Mega-Science, CAS Center for Influenza Research and Early Warning, Chinese Academy of Sciences, Wuhan 430071, China
*Equal contribution

Correspondence to: Congqing Jiang, Xiaoyu Xie; **email:** wb002554@whu.edu.cn, zn004356@whu.edu.cn
Keywords: slow transit constipation, miR-128, M-CSF, inflammation
Received: September 25, 2020 **Accepted:** January 14, 2021 **Published:**

ABSTRACT

Slow transit constipation (STC) is a gastrointestinal disorder that adversely affects the quality of life. MicroRNAs are involved in the pathogenesis of functional gastrointestinal disorders. This study aims to investigate the molecular mechanism of microRNA-128 in STC. Here, we successfully constructed a murine model of STC based on morphine and rhubarb. The expression of stem cell factor (SCF) and neuron-specific enolase (NSE) were low in the models. Using miRNA array and bioinformatic analysis, we predicted and confirmed the expression of miR-128 and its downstream target genes in STC model. Compared to the control group, STC group showed a significant downregulation of miR-128 and upregulation of p38α and macrophage colony stimulating factors (M-CSF). Moreover, we observed elevated inflammatory cytokine and decreased anti-inflammatory cytokine levels in colonic tissues. Furthermore, co-culture assays indicated that regulating expression of miR-128 in colonic epithelial cells induced the secretion of IL-6 and TNF-α by macrophages. In conclusion, our study demonstrated that miR-128 regulated the p38α/M-CSF signaling pathway to promote chronic inflammatory responses and changes in the immune microenvironment of the colon, thereby offering potential insights into the pathogenesis of STC and therapeutic targets for its treatment.

INTRODUCTION

Chronic constipation is a functional gastrointestinal disorder that severely affects the physical and mental health, and quality of life of people in modern societies. In particular, slow transit constipation (STC) is a common type of chronic intractable constipation characterized by delayed colonic transit and accounts for 10.3% to 43.5% of all chronic constipation cases [1]. Research shows that STC might play a pivotal role in

the onset of disorders, such as colorectal cancer, cardiovascular and cerebrovascular disease, Alzheimer's disease, bowel obstruction, rectal prolapse, and anal fissure [2–6]. However, the mechanisms associated with STC pathogenesis have not yet been fully elucidated, and the current chronic constipation-treatments suffer from the drawbacks such as long treatment duration and poor overall therapeutic effects.

MicroRNAs (miRNAs) are a class of small noncoding RNAs that play essential roles in many physiological and pathological processes, including inflammation and cell proliferation. miRNAs (including miR-128) have been shown to be involved in the pathogenesis of functional gastrointestinal disorders via the regulation of the morphologies and functions of interstitial cells of Cajal (ICCs) and smooth muscle cells (SMCs) in the intestinal tract [7–9]. In our previous study, we performed gene-expression analysis of miR-128 in the colonic tissues of STC patients. We found that the expression of miR-128 and miR-129-3p were significantly downregulated in the STC colonic tissue. In addition, miR-128 expression was significantly positively correlated with c-kit (CD117) and smoothelin levels and significantly negatively correlated with the number of inflammatory cells. Therefore, we speculated that changes in miR-128 expression in the colonic epithelium might be associated with STC pathogenesis [10].

There has been an increasing interest in the role of inflammation and inflammatory cells in the pathogenesis of gastrointestinal motility disorders worldwide. Numerous studies on gastrointestinal disorders in patients and animal models have revealed that cytokines [e.g., tumor necrosis factor (TNF)-α, interleukin (IL)-6 and monocyte chemoattractant protein-1 (MCP-1)] secreted by macrophages (especially submucosal resident macrophages) and mast cells after infiltration and activation in the gastrointestinal tract can directly or indirectly damage the ICCs or SMCs in the gastrointestinal tract, thereby aggravating the gastrointestinal motility impairment or disorder [11–14]. The number of infiltrating inflammatory cells (including macrophages and mast cells) is significantly higher in the colonic tissue of patients with STC than that in the normal colonic tissue. In our previous study, we found a decreased ICC count and increased macrophages infiltration in the submucosal border of the circular muscle layer and the internal circular muscle layer of colonic tissue samples of patients with STC. Additionally, increased macrophage-colony stimulating factor (M-CSF) expression and the negative correlation between macrophage number and miR-128 expression were indicative of inflammatory cell infiltration in the colonic tissues of patients with STC [10].

In the present study, we investigated whether M-CSF is regulated by miR-128 and elucidated the mechanisms involved in the expression and regulation of inflammatory cytokines in the STC colonic tissue.

RESULTS

Successful construction of cathartic colon STC model

The barium enema experiment confirmed the presence of significantly slower colonic transit ($p < 0.05$; Figure 1A, 1B) in the rhubarb and morphine+rhubarb groups. Compared with the saline group, mice that only received subcutaneous injections of morphine also exhibited a delay in colonic transit. This represented a case of morphine simulation of gastrointestinal disorders similar to that observed in case of chronic laxative use by STC patients.

Additionally, comparisons of the gross appearance and water content of stool samples collected from the mouse models revealed that the morphine+rhubarb group had significantly drier and smaller stools with a significantly lower water content compared to the morphine group (Figure 1C). Taken together, we have successfully established a cathartic STC mouse model based on morphine and rhubarb.

Hematoxylin and eosin (HE) staining of colonic tissues (Figure 2A) revealed that the morphine group exhibited clear structures in the various colonic tissue layers, and regular and organized arrangement of muscle fibers, which did not differ significantly from the saline group. However, both the rhubarb group and morphine+rhubarb group exhibited thinner circular muscle-layer structures and poor structural damage in the colonic mucosal tissue relative to the saline group (Figure 2A). As the characteristics of the morphine+rhubarb group were more similar to the characteristics of disease progression observed in patients with STC, we defined the morphine+rhubarb group as the STC group and the morphine group as the control group for subsequent analyses.

Enteric nerve injury in the STC model

Stem cell factor (SCF) was used as the marker for slow wave-generating ICCs in the gastrointestinal tract and neuron-specific enolase (NSE) was a key marker of the enteric nervous system (ENS). In our cathartic colon model, both protein and gene-expression levels of NSE and SCF were significantly decreased in the STC group as compared with those in the morphine group ($p < 0.05$; Figure 2B–2D). Additionally, the expression of ICC marker TMEM16A decreased in the submucosal

border (SMB) of the circular muscle layer, and the internal circular muscle (CM) layers in STC group (Supplementary Figure 2). Taken together, decreased ICC count and developmental and functional disorders of the ENS were observed in the cathartic colon model.

Decreased miR-128 expression and prediction of downstream target genes in the STC model

Changes in miRNA expression in the morphine and STC groups were measured using the miRNA array. The expression of 12 miRNAs was downregulated (including miR-193a-5p) and that of 45 miRNAs was upregulated (including miR-134-5p) (Figure 3D). Subsequent qPCR revealed that miR-128-2-5p expression in the STC group was significantly decreased compared to that in the morphine group (p<0.05; Figure 3C). These results confirmed the downregulation of miR-128-2-5p in the STC mouse model, a result that is consistent with our previous findings in STC patients.

To predict the downstream target genes of miR-128, we analyzed five miRNA databases (i.e., TargetScan, PicTar, miRanda, microT, and miRmap); 264, 676, 1439, 1138, and 1319 target genes were identified using

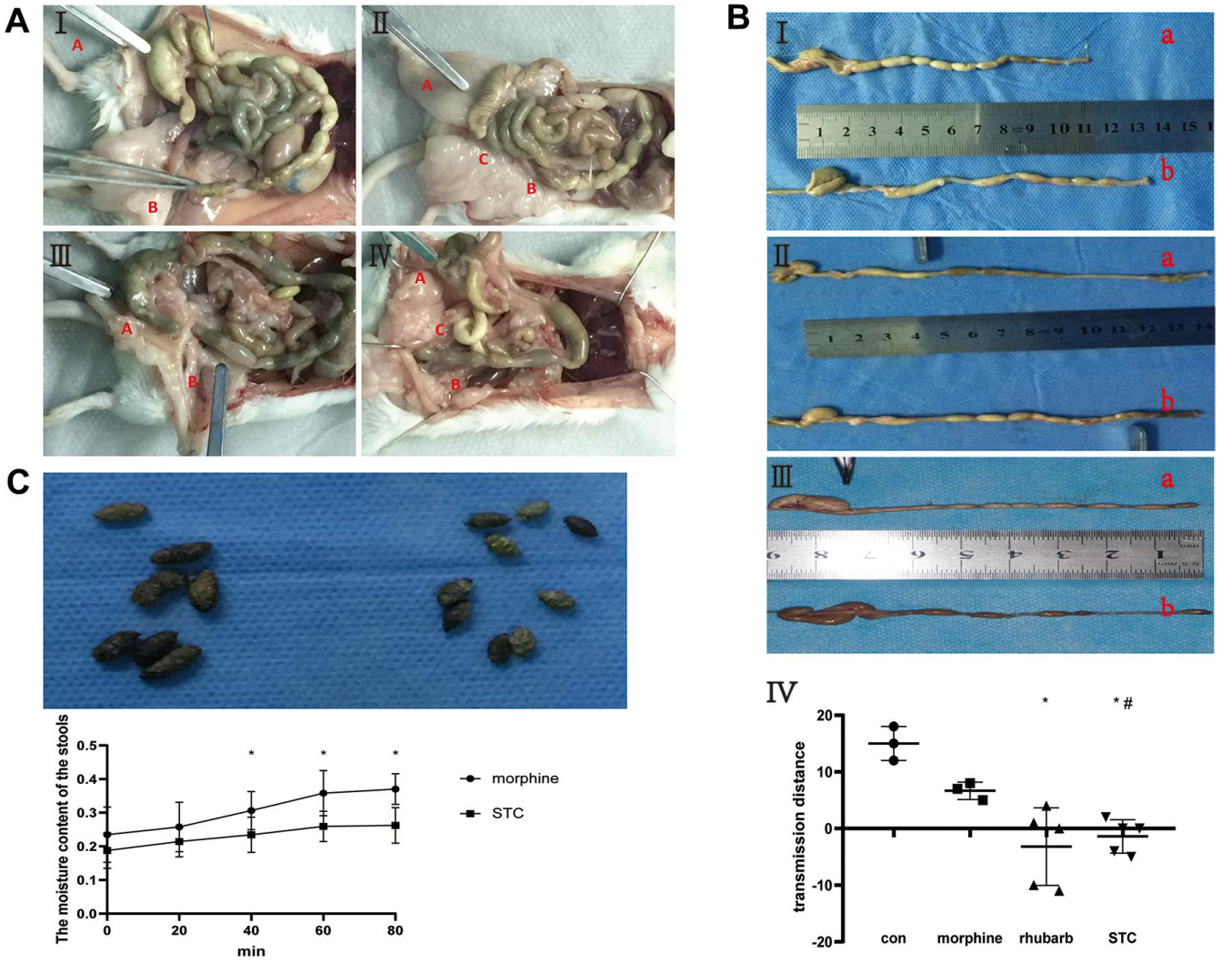

Figure 1. Construction of cathartic colon mice models. (**A**) anatomical appearance of four groups. *I* saline group, *II:* morphine group, *III* rhubarb group, *IV* morphine+rhubarb group; *Red A* vermiform appendix, *Red B* rectum, *Red C* anus. (**B**) measurement of stool-transit distance after barium enema examination. *I* saline group (**a**) vs morphine group (**b**), *II* saline group (**a**) vs rhubarb group (**b**), *III* morphine group (**a**) vs morphine+rhubarb group (**b**), *IV* measurement of stool-transit distance; the forceps show the positions of transit barium, *p<0.05, versus saline group; #p<0.05, versus morphine group. (**C**) collection of stool samples. *I* appearance of stools in morphine group(L) and morphine+rhubarb group (R), *II* dynamic changes of the moisture content of stools in 65° C oven.

TargetScan, PicTar, miRanda, microT, and miRmap, respectively. A Venn diagram revealed that 56 target genes [including *mitogen-activated protein kinase* (*Mapk*)*14*] were common across all five databases (Figure 3A). Enrichment analysis of these predicted miR-128-target genes using starBase revealed a greater distribution of genes within the MAPK signaling pathway, suggesting that the MAPK pathway was a key downstream pathway affected by miR-128 (Figure 3B).

miR-128 regulates the p38α/M-CSF signaling pathway

The p38 MAPK plays an essential role in responding to environment stress and contributes to the pathology of inflammation. Measurement of p38α and M-CSF expression in the colonic tissues by western blotting indicated significantly higher p38α and M-CSF levels in STC group relative to those in the morphine group ($p < 0.05$; Figure 3E). Additionally, qPCR indicated

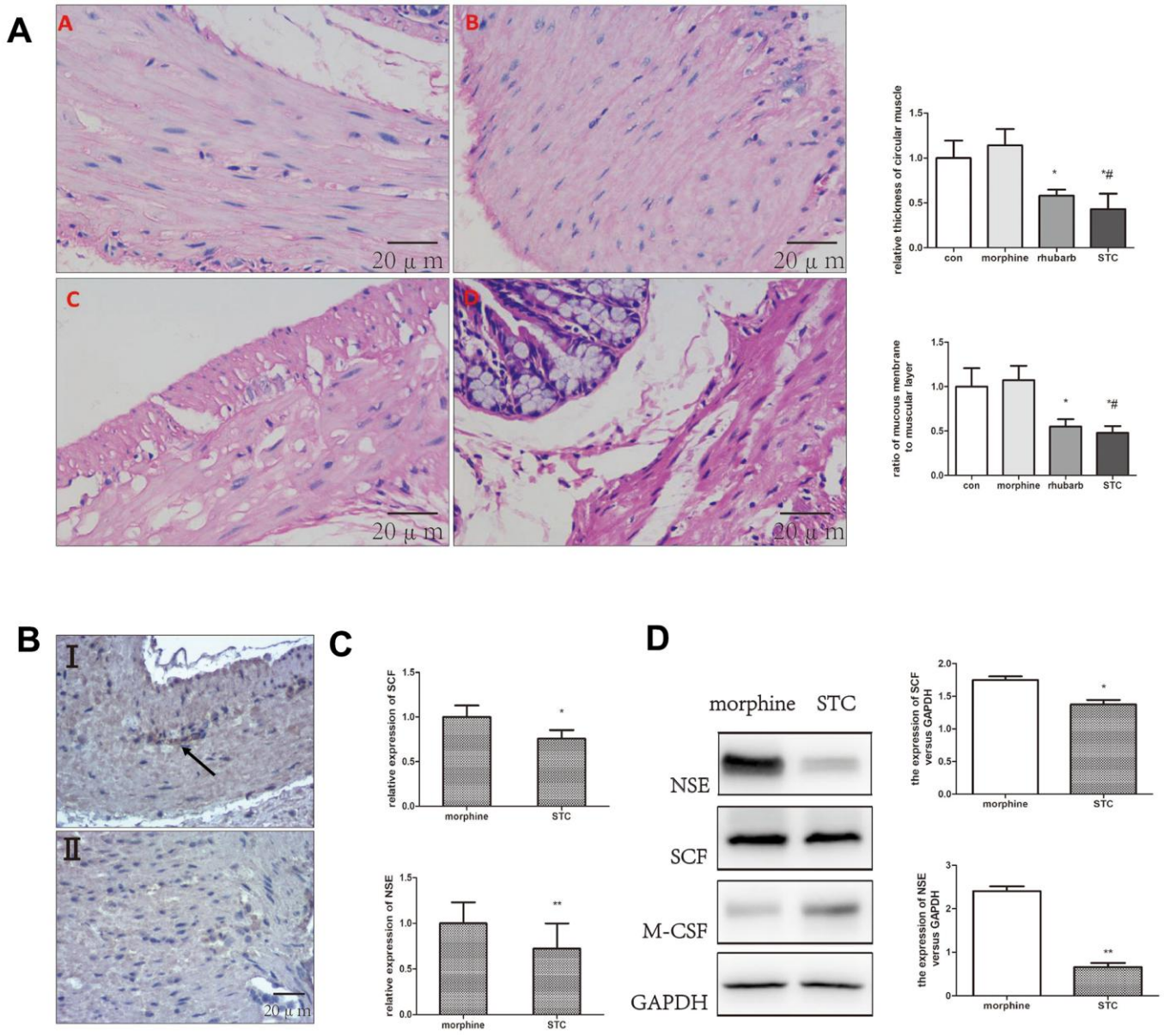

Figure 2. Differential expression of SCF, NSE in colonic samples. (**A**) HE staining performed on colonic tissues [original magnification ×40]. saline group (**A**), morphine group (**B**), rhubarb group (**C**), morphine+rhubarb group (**D**). (**B**) IHC staining (anti-SCF) performed on colonic tissues [original magnification ×40]. *I* morphine group, *II:* morphine+rhubarb group (STC). (**C**) the mRNA expression of SCF, NSE expression in cathartic colon mice models. (**D**) the protein expression of SCF, NSE in cathartic colon mice models. **P*<0.05 versus saline group, #*P*<0.05 versus morphine group.

significantly upregulated M-CSF expression in the STC group ($p < 0.05$; Figure 3F), whereas p38α expression did not differ significantly different between the two groups.

To elucidate the effects of miR-128 on p38α/MAPK and the downstream genes encoding AKT and M-CSF, we separately trans-infected CT26.WT cells with the micrON mmu-miR-128-2-5p mimic, micrON-mimic NC, micrOFF mmu-miR-128-2-5p inhibitor, and micrOFF-inhibitor NC. Successful and effective trans-infection was confirmed by measuring post-transfection miR-128-2-5p expression (Figure 4A, 4C). In cells trans-infected with the mmu-miR-128-2-5p mimic, qPCR analysis revealed that expression of p38α, AKT and M-CSF decreased significantly ($p < 0.05$; Figure 4B). Subsequent confirmation by western blotting revealed significant decrease in p38α and M-CSF protein levels along with an increase in miR-128-2-5p expression ($p < 0.05$). The trans-infection of the mmu-miR-128-2-5p inhibitor significantly increased the expression of p38α, AKT and M-CSF ($p < 0.05$; Figure 4D). Subsequent confirmation by western blotting revealed a significant increase in p38α and M-CSF levels ($p < 0.05$; Figure 5E).

These results showed that the expression of miR-128 decreases in the STC model, and the treatment with miR-128 mimics and inhibitors confirmed that miR-128-2-5p negatively regulates the p38α/AKT/M-CSF pathway.

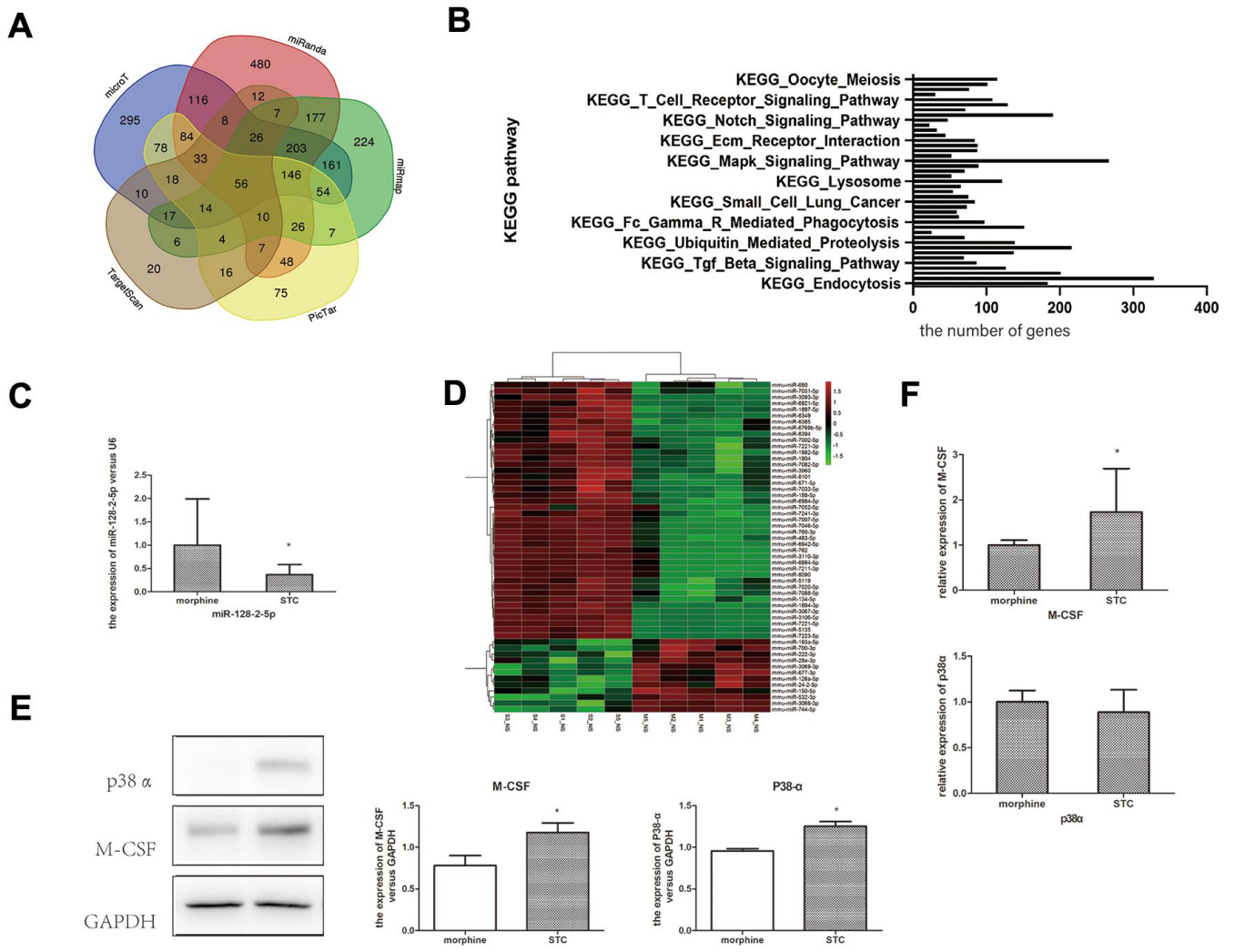

Figure 3. Confirmation miR-128 expression and prediction of downstream target genes in STC model. (**A**) The venn diagram showing the overlapping genes among databases. (**B**) KEGG pathway enrichment of miR-128 interactive genes. (**C**) the mRNA expression miR-128-2-5p in cathartic colon mice models. (**D**) heat map show the up-regulated and down-regulated miRNAs in cathartic colon mice models. (**E**) the mRNA expression p38α, M-CSF in cathartic colon mice models. (**F**) the protein expression of p38α, M-CSF in cathartic colon mice models. **P*<0.05.

miR-128-induced effects of M-CSF in colonic epithelial cells on colonic macrophages

Next, we measured the levels of the pro-inflammatory cytokines IL-6, IL-8, and TNF-α and anti-inflammatory cytokines IL-10 and transforming growth factor (TGF)-β in the colonic tissues of the morphine and STC groups to determine inflammation levels in the cathartic colon model Supplementary Figure 1. qPCR revealed significantly elevated *Il6* and *Il8* expression, significantly decreased TGF-β expression, and no significant changes in TNF-α or IL-10 expression in STC group compared with those in morphine group ($p < 0.05$; Figure 5A). However, at the protein level, TNF-α level increased significantly ($p < 0.05$), whereas IL-6 expression did not change significantly relative to the morphine group (Figure 5B). Measurement of apoptosis-related markers in the tissue samples revealed a significant downregulation of B-cell lymphoma-2 (Bcl-2) levels in STC mice but no significant changes in Bax or Caspase-3 levels, suggesting that STC pathogenesis is unrelated to apoptosis (Figure 5C). These results indicated that the chronic effects of rhubarb might lead to the release of substantial quantities of inflammatory mediators in intestinal tissue, which is indicative of the inflammatory status of the colonic tissue.

To determine the miR-128-induced effects of M-CSF in colonic epithelial cells on colonic macrophages, we co-cultured CT26.WT together with RAW246.7 cells. Compared with the untreated NC group, CT26.WT cells trans-infected with the miR-128 inhibitor showed a significant increase in M-CSF levels in the supernatant ($p < 0.01$), whereas cells transfected with the miR-128

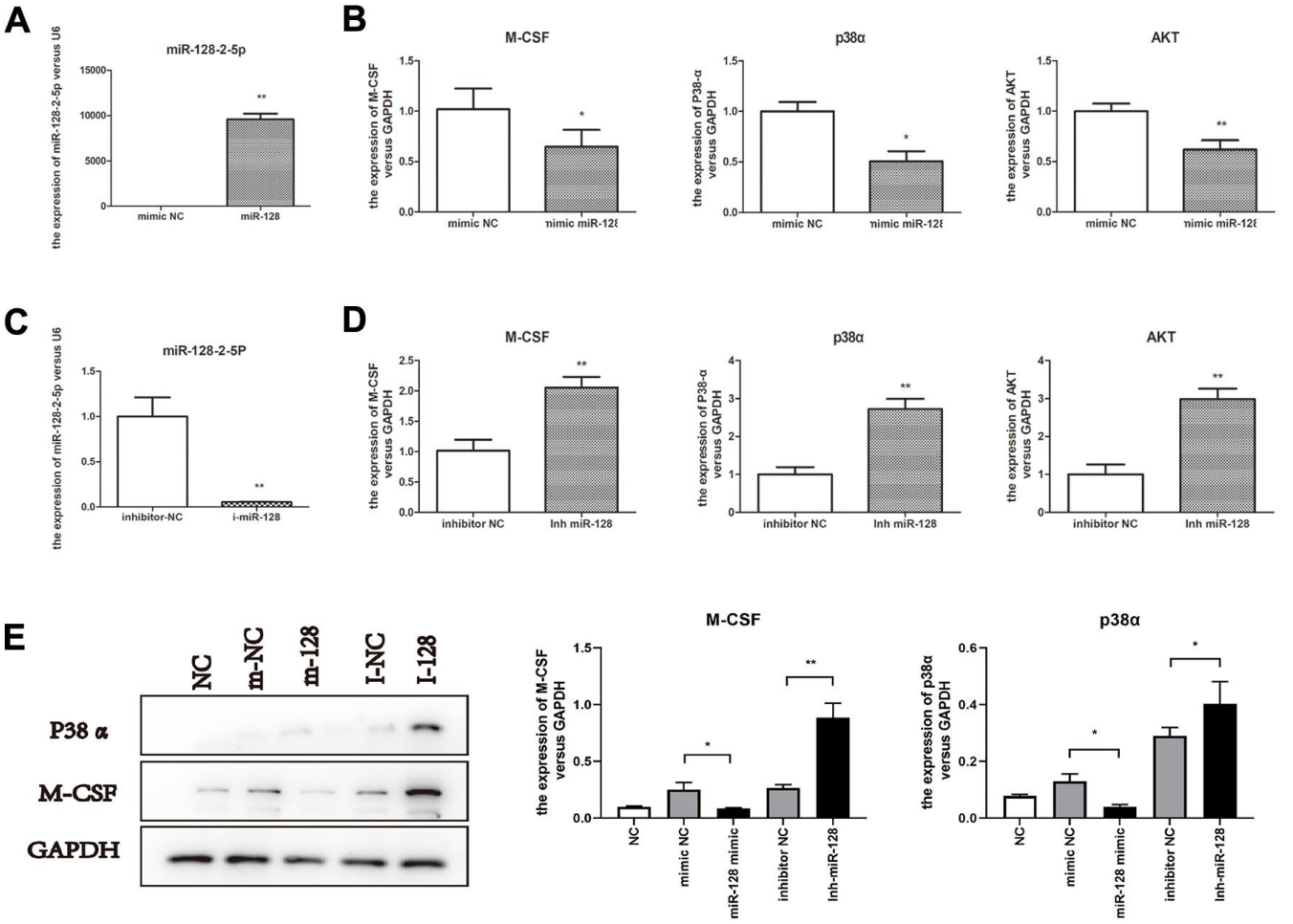

Figure 4. miR-128 interference in CT26.WT cells affect expression of miR-128 toward p38α/MAPK and the downstream genes AKT and M-CSF. (**A**, **B**) miR-128-2-5p, M-CSF, p38α and AKT mRNA expression levels in cells trans-infected with micrON mmu-miR-128-2-5p mimic/micrON mimic NC; (**C**, **D**) miR-128-2-5p, M-CSF, p38α and AKT mRNA expression levels in cells trans-infected with mmu-miR-128-2-5p inhibitor/ micrOFF inhibitor NC. (**E**) protein expression levels of M-CSF, p38α in CT26.WT cells trans-infected with micrON mmu-miR-128-2-5p mimic/micrON mimic NC/ micrOFF mmu-miR-128-2-5p inhibitor/ micrOFF inhibitor NC. **P*<0.05, ***P*<0.01.

mimic showed a significantly lower M-CSF levels in the supernatant relative to cells transfected with mimic NC ($p < 0.05$). ($p < 0.05$; Figure 6B). Moreover, measurement of TNF-α, IL-6 in the RAW264.7 cells indicated that compared with the mimic NC group, the miR-128-mimic group showed lower levels of TNF-α and IL-6, ($p < 0.05$), whereas RAW264.7 cells of the miR-128-inhibitor group showed significantly higher levels of TNF-α and IL-6 relative to the inhibitor NC group ($p < 0.05$; Figure 6A). Western blotting showed results similar to those observed for TNF-α and IL-6 expression in RAW264.7 cells (Figure 6C).

These results demonstrated that changes in M-CSF expression induced by changes in miR-128 levels in the colonic epithelium might promote altered expression of inflammatory mediators in colonic macrophages, which could ultimately lead to the onset of inflammation due to the increased expression of proinflammatory cytokines, such as IL-6 and TNF-α Supplementary Figure 3.

DISCUSSION

In recent years, numerous approaches have been adopted for the development of constipation models. Based on the principle of model establishment, model-construction methods can be classified as water-restriction, ice-water-gavage, cathartic colon, and drug-administration methods [15]. As chronic constipation patients in China primarily depend on laxatives

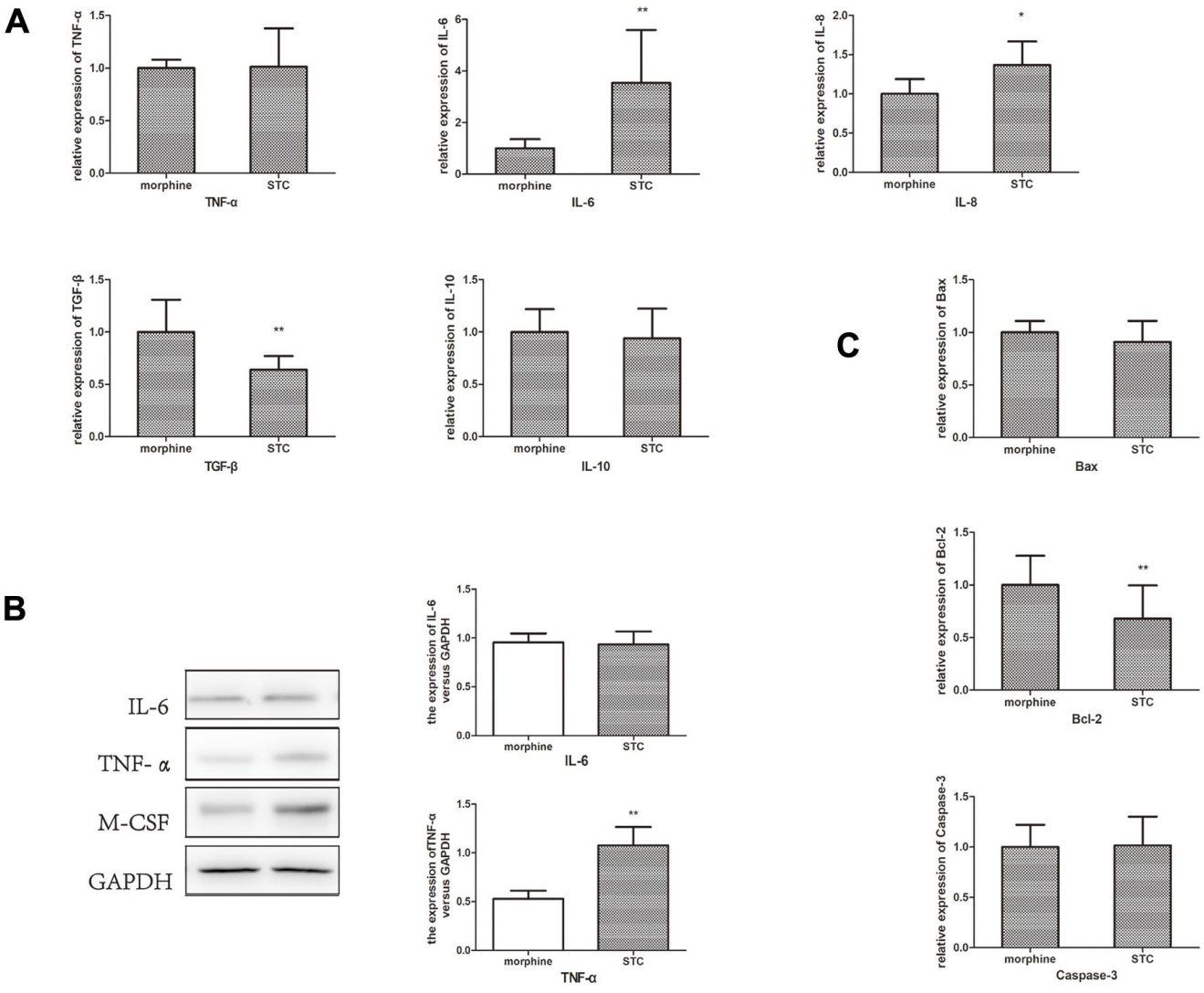

Figure 5. Measurement of the inflammatory cytokines, anti-inflammatory cytokines and apoptosis-related markers. (**A**) mRNA expression of IL-6, IL-8, TNF-α, IL-10 and TGF-β in STC model. (**B**) The protein expression levels of IL-6 and TNF-α. (**C**) mRNA expression of Bax, Bcl-2 and Caspase-3 in STC model. **P*<0.05, ***P*<0.01.

containing rhubarb as the active ingredient for the alleviation of constipation symptoms, and because the construction of a rat model of cathartic colon using rhubarb and phenolphthalein had been described in a previous study [16], we attempted to construct a mouse model of STC through the combined use of rhubarb and morphine.

Morphine is a widely used opioid analgesic, with constipation being one of the most common adverse gastrointestinal effects of morphine use. A previous study found that acute gastrointestinal transit dysfunction can occur as early as 20 min after intraperitoneal injection of morphine [17]. Activation of the μ-opioid and δ-opioid receptors in the gastrointestinal tract can inhibit the release of motor neurons from the submucosal plexus, thereby reducing chloride-dependent water transport into the intestinal cavity. Consequently, the intestinal contents become dehydrated, resulting in harder and drier stools. Additionally, activation of μ-opioid receptors leads to the generation of stronger and more frequent non-propagating contractions by the circular muscle layer of the gastrointestinal tract, which promotes the re-absorption of liquid within the intestinal cavity and reduces baseline muscle tone, thereby resulting in harder and drier stools, reduced intestinal contractility, and prolonged bowel transit time [18]. Moreover, activation of μ-opioid receptors increases the muscle tone in the anal sphincter, which causes further difficulties in stool passage and can trigger acute constipation [19].

Given the acute constipation-inducing effects of morphine, we subcutaneously administered morphine into mice at the initial stage of cathartic colon model construction. After acute morphine administration, the stool-transit distance decreased significantly (−0.9 cm vs. 2.4 cm), suggesting the presence of an acute gastrointestinal disorder in the mice. However, after morphine injections had been stopped, and rhubarb had been subsequently administered in drinking water for 120 days, we found that morphine no longer served as an influencing factor of gastrointestinal transit function (Figure 1B). During the model-construction process, subcutaneous morphine injections provided a realistic simulation of the acute constipation experienced by clinical patients prior to laxative use, which resembled the characteristics of STC encountered in clinical practice. Therefore, the morphine+rhubarb group was defined as the STC model, and subsequent investigations were performed on the basis of this model.

miR-128 is a highly conserved miRNA present in the genomes of humans and rodents, suggesting that it possesses functions associated with cell regulation [20, 21]. Previous studies have reported that miR-128 acts as

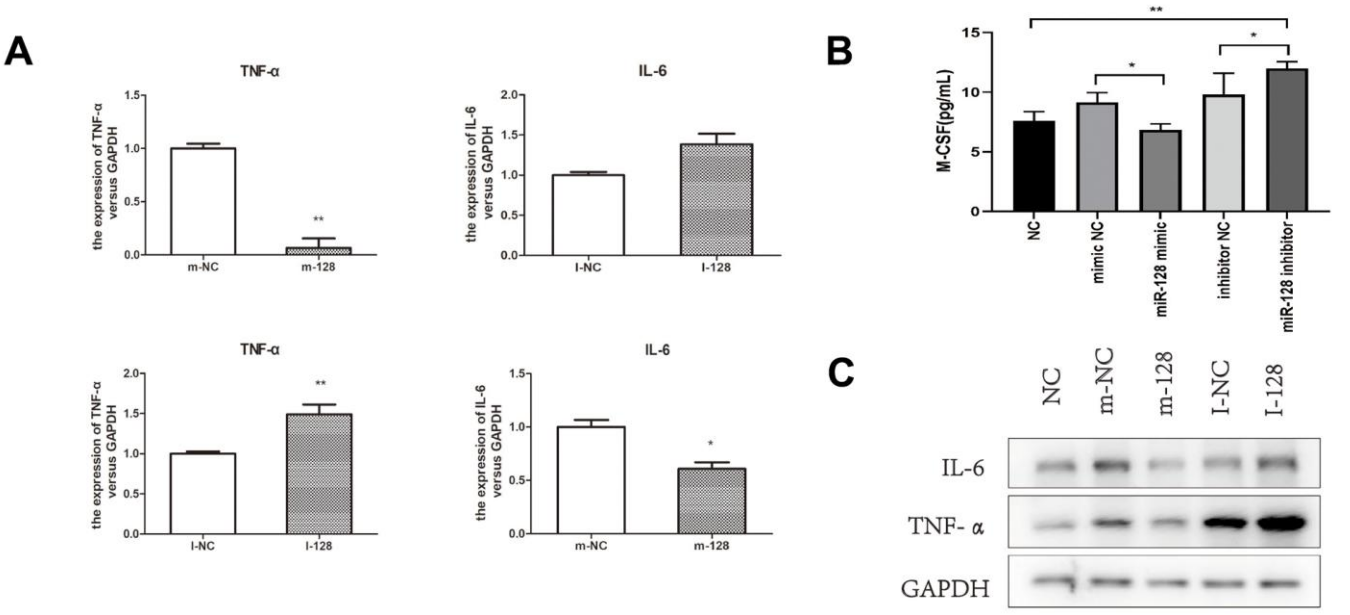

Figure 6. The results of co-culturing RAW264.7 cell CT26.WT cell. (**A**) The mRNA expression levels of IL-6 and TNF-α in RAW264.7 cells after co-culturing. (**B**) M-CSF level in the supernatant after trans-sfected with the miR-128 mimic/inhibitor. (**C**) The protein expression levels of IL-6 and TNF-α in RAW264.7 after co-culturing. I-NC, micrOFF inhibitor NC; I-128, micrOFF mmu-miR-128-2-5p inhibitor; m-NC, micrON mimic NC; m-128, micrON mmu-miR-128-2-5p mimic. **P*<0.05, ***P*<0.01.

a tumor suppressor in breast and lung cancer [22, 23] and is enriched in brain tissue [24]. These findings suggest that miR-128 plays different roles in human growth and disease development. In the present study, we measured mmu-miR-128 expression in the cathartic colon mouse model using miRNA array and qPCR, revealing a significant decrease in mmu-miR-128 expression.

The MAPK pathway is a key regulator of cell proliferation, differentiation, and apoptosis in eukaryotes. A previous study showed that miR-128 can regulate MAPK signaling in neuropsychiatric diseases and tumor tissues [24]. Among the four subtypes of the gene encoding p38 (α, β, γ, and δ), the p38α subtype encoded by *MAPK14* is widely expressed in various tissue types [25]. Transfection of NRT cells with an miR-128 mimic downregulated the expression of genes which were the direct targets of miR-128, including *MAPK14* [21]. In the present study, we predicted p38α as a downstream target of mmu-miR-128 using multiple miRNA databases and subsequently trans-infected CT26.WT cells with an mmu-miR-128-2-5p mimic and mmu-miR-128-2-5p inhibitor. The results showed that mmu-miR-128-2-5p exerted negative regulatory effects on the p38α/AKT pathway, suggesting that decreased expression of miR-128 upregulated p38α/AKT activity in the STC process.

M-CSF plays an essential role in regulating the mature myeloid cell populations in the steady state and during inflammation. M-CSF is secreted by multiple cell types, including endothelial cells, osteoblasts, SMCs, fibroblasts, and macrophages. In a disease state (e.g., cancer, inflammation or autoimmune disease), the M-CSF level in blood circulation is increased. Studies show that M-CSF is associated with the onset of many types of diseases, with increased M-CSF levels in blood circulation observed in patients with arthritis, nephrotic syndrome, pulmonary fibrosis, obesity, inflammatory bowel disease, and metastatic cancer [26, 27]. Additionally, animal experiments indicate that the reduction (neutralization) of M-CSF or blockade of M-CSF-R decreases the severity of inflammation, autoimmune disease, and cancer [28, 29]. Multiple studies conducted on mouse models of lupus nephritis report that M-CSF causes renal inflammation, and that a systemic increase in M-CSF leads to acceleration of disease onset and progression [30, 31]. Furthermore, M-CSF plays a key role in gastrointestinal inflammation, with M-CSF-regulated interactions between muscularis macrophages and enteric neurons co-regulating gastrointestinal motility [32]. In a study on the immune-escape mechanism of Salmonella, increased miR-128 expression reduced M-CSF secretion from colonic epithelial cells, thereby reducing macrophage chemotaxis and controlling the progression of inflammation [33]. In the present study, we found that miR-128 overexpression results in the downregulation of M-CSF and attenuated miR-128 expression results in upregulation of M-CSF in colonic epithelial cells.

Macrophage recruitment at sites of inflammation is primarily induced by proinflammatory cytokines, such as M-CSF and MCP-1. Macrophage differentiation and survival are also closely associated with M-CSF [34–36]. Hoi et al. [34] showed that M-CSF secreted by epithelial cells promotes macrophage recruitment by inducing inflammation. In the present study, our findings provided direct proof that changes in miR-128 expression in epithelial cells induced changes in downstream M-CSF level. Moreover, these results were verified by measurement of M-CSF levels in cell cultures subjected to miR-128 interference, thereby indicating that miR-128 exerts anti-inflammatory effects during the progression of inflammation.

Furthermore, to determine whether inflammation in mouse colonic tissue was associated with miR-128, we co-cultured mouse colonic epithelial cells with mouse macrophages using Transwell inserts, and utilized miR-128-2-5p mimic and miR-128-2-5p inhibitor for miRNA interference in the colonic epithelial cells. We observed significant changes in M-CSF-R, IL-6, and TNF-α levels in macrophages in the bottom layer, suggesting that miR-128 in the colonic epithelial cells induced alterations in inflammatory cytokine release by macrophages via its influence on M-CSF.

In conclusion, our study demonstrated that reduction in miR-128 levels enhanced the expression and release of M-CSF in colonic epithelial cells by targeting p38α, promoted inflammatory cell (i.e., macrophages) infiltration, and increased inflammatory cytokine expression in the colonic tissue. This activity resulted in chronic inflammatory response and changes in the immune microenvironment of the colon, thereby causing ICC and enteric nerve injury and ultimately contributing to STC pathogenesis, and it might offer potential therapeutic targets for its treatment. Further investigation is required to determine whether macrophages influence ICCs and the relevant associated mechanisms when changes occur in miR-128 expression in colonic tissue.

MATERIALS AND METHODS

Cells and culture

The mouse colorectal carcinoma cell line CT26.WT (RRID: CVCL-7256) and mouse monocyte/macrophage cell line RAW264.7 were purchased from ATCC

(Manassas, VA, USA). RPMI 1640 medium, 10% fetal bovine serum, and 1% penicillin-streptomycin were used for cell culture.

miRNA interference

The following miRNA interferents were purchased from Guangzhou RiboBio Co., Ltd. (Guangzhou, China): micrOFF mmu-miR-128-1-5p inhibitor, micrOFF mmu-miR-128-2-5p inhibitor, micrOFF-mimic NC, micrON miR-128-1-5p mimic, micrON miR-128-2-5p mimic, and micrON-mimic NC. CT26.WT cells were separately transfected with the aforementioned interferents and miR-NC using Lipofectamine 2000 (Thermo Fisher Scientific, Waltham, MA USA). At 72-h post-transfection, cells were collected for use in subsequent experiments.

Animal models

128 SPF-grade ICR female mice were purchased from Hubei Provincial Center for Disease Control and Prevention (Wuhan, China) and randomly allocated to the morphine group and untreated group. Model construction was performed over a 1-week period by daily subcutaneous injections of 10 mg/kg morphine for the morphine group and equivalent volumes of saline for the untreated group. Subsequently, mice were randomly selected from the two groups and subjected to barium enema examination for the measurement of stool-transit distance. The model construction took more than 4 months. Following establishment of the morphine-stimulated acute STC model, mice in the untreated group were randomly sub-divided into the control group and rhubarb group, and mice in the morphine group were randomly sub-divided into the morphine group and morphine+rhubarb group. The rhubarb group and morphine+rhubarb group were administered rhubarb decoction in drinking water starting from a dose of 300 mg/kg•day (~5 mL/day based on the average body weight of the mice). Rhubarb was extracted from natural rhubarb, the rhubarb was concentrated to 1 g/mL using a 40 degree water bath. The dose of rhubarb decoction was doubled daily until ~50% of the mice exhibited loose stools at a dose of 2000 mg/kg•day. Subsequently, the dose level was maintained until >80% of the mice no longer exhibited loose stools, which occurred on day 107 of rhubarb administration. After the rhubarb decoction had been administered for 120 days, mice were randomly selected and subjected to barium enema examination to measure stool-transit distance. 2mL 60% (W/V) Barium Sulfate for Suspension (Type I) (Shengli Co., Ltd, Shandong, China) was injected to stomach through oral gavage for stool-transit measurement. The transmission of barium was measured 2 hours after injection and ileocecum was defined as the starting position of colonic transmission. The stools of the mice were collected, dried in a 65° C oven, and weighed every 20 min in a cryopreservation tube. When the mass of the stool sample no longer changed, the dry weight of stools was calculated as total weight − cryopreservation tube weight, and the moisture content of the stools was calculated as (wet weight of stools − dry weight of stools) / wet weight of stools × 100%.

Experiments were performed under a project license (No.2018039) granted by the ethics committee of Zhongnan Hospital of Wuhan University, Wuhan, China, in compliance with Animal Research Center of Wuhan University guidelines for the care and use of animals.

Immunohistochemistry (IHC)

The tissues were fixed in 10% neutral buffered formalin and then subjected the 5μm thick slices were subjected to heat-induced epitope retrieval by immersion in a heat-resistant container filled with citrate buffer solution (pH 6.0), placed in a pressure cooker, and microwaved for 20 min. Endogenous peroxidase activity was blocked by employing 3% H_2O_2 incubation for 5 min. M-CSF staining (rabbit monoclonal antibody against M-CSF, ab233387, dilution 1:500; Abcam, Inc., Cambridge, MA, USA) was used to evaluate the number of stromal cells. The number of mast cell was evaluated using anti-Mast Cell Tryptase (rabbit monoclonal antibody against mast cell tryptase, ab151757, dilution 1:100; Abcam, Inc., Cambridge, MA, USA). ICCs were detected using the ICC marker SCF (rabbit polyclonal antibody against SCF, 26582-1-AP, dilution 1:100, Proteintech Group, Inc, IL, USA) and TMEM16A (rabbit polyclonal antibody against TMEM16A, 12652-1-AP, dilution 1:50, Proteintech Group, Inc, IL, USA). The number of positive cells was calculated and expressed as the mean number of the results from all slides. HMIAS-2000 (Wuhan, China) imaging system was used for recording.

Real-time fluorescence-based quantitative PCR (qPCR)

Total RNA was extracted using TRIzol reagent (Invitrogen, Carlsbad, CA, USA) and reverse transcribed into cDNA. qPCR was performed using U6 and *glyceraldehyde 3-phosphate dehydrogenase* (*GAPDH*) as reference genes to measure relative changes in the expression of miRNA and target genes. miRNA expression was measured using a Taqman assay under the following PCR amplification conditions: initial denaturation at 50° C for 2min and 95° C for 10 min, followed by 45 cycles of denaturation

at 95° C for 15s, and annealing at 60° C for 60s. Gene expression was measured using SYBR Green under the following PCR amplification conditions: initial denaturation at 95° C for 30s, followed by 40 cycles of denaturation at 95° C for 30s, annealing at 60° C for 30s, and extension at 72° C for 30s.

Primer sequences for qPCR were obtained from the GenBank and miRbase databases, and the primers were designed using Primer Premier 5 (Premier Biosoft, San Francisco, CA, USA). The sequences of the primers are shown in Supplementary Table 1.

Western blotting

Total protein was extracted from cells and tissues using a lysis buffer. After volume adjustment, the total protein was resolved via sodium dodecyl sulfate polyacrylamide gel electrophoresis and transferred to a methanol-activated polyvinylidene difluoride membrane (Millipore Sigma, Billerica, MA, USA). The membrane was incubated with antibodies, and the protein was visualized based on enhanced chemiluminescence, with GAPDH used as a loading control. The primary antibody (Supplementary Table 2 for detailed antibody information) and secondary antibody (Abcam Cat# ab6728, RRID: AB-955440) were purchased from Abcam (Cambridge, MA, USA). Experimental results were processed using ImageJ software (National Institutes of Health, Bethesda, MD, USA).

Enzyme-linked immunosorbent assay (ELISA)

Mouse TNF-α and IL-6 ELISA kits were purchased from Proteintech (Proteintech Group, Rosemont, IL, USA). Equivalent amounts of mouse colonic tissue were weighed, washed with phosphate-buffered saline, and sufficiently homogenized. The supernatant was then obtained for the measurement of TNF-α (Cat No. KE10002) and IL-6 (Cat No. KE10007) levels according to the manufacturer's instructions.

Cell co-culturing

Cells were co-cultured using 0.4-μm pore size Transwell inserts, with CT26.WT cells in the top layer and RAW246.7 cells in the bottom layer. Samples were collected for testing after the co-culturing of CT26.WT cells that had been subjected to miRNA interference with RAW264.7 cells for 48 h.

Statistical analysis

Data analysis was performed using GraphPad Prism software (v.8.0; GraphPad Software, La Jolla, CA, USA). All data were expressed as the mean±standard deviation. Differences in miRNA array data were calculated using the limma algorithm, with an adjusted $p < 0.05$ and $-1 \leq$ fold change ≤ 1 used as thresholds, and differences in miRNA between groups were compared using Student's *t* test. $p < 0.05$ was considered statistically significant.

Abbreviations

STC: slow transit constipation; M-CSF: macrophage-colony stimulating factor; SCF: stem cell factor; NSE: neuron-specific enolase; MAPK: mitogen-activated protein kinase; ICCs: interstitial cells of Cajal; SMCs: smooth muscle cells; MCP-1: monocyte chemoattractant protein-1.

AUTHOR CONTRIBUTIONS

CQJ and XYX conceptualized and designed the study. YTH, WCL, BL, XHR, KLS, XQY and XYX conducted the experiments. XYX, YTH, WCL and BL analyzed and interpreted the data. WCL, XHR and XQY contributed to the sample collection. CQJ and QQ provided technical support. YTH, XYX and CQJ wrote and revised the manuscript. All authors read and approved the final manuscript.

CONFLICTS OF INTEREST

The authors declare no conflicts of interest.

FUNDING

This work was supported by grants from the National Natural Science Foundation of China (No.81570492, No.81500505), Science and Technology Innovation Fostering Foundation of Zhongnan Hospital, Wuhan University (cxpy2017018), Medical Science and Technology Innovation Platform of Health Commission of Hubei Province / Zhongnan Hospital of Wuhan University (No.PTXM2019011), Health Commission of Hubei Province (No. WJ2019M206), Science and Technology Department of Hubei Province (No.2018CKB913), and the Clinical Research Special Fund of Wu Jieping Medical Foundation (No.320.6750.18467, No.320.6750.19089-14).

REFERENCES

1. Bharucha AE, Wald A. Chronic constipation. Mayo Clin Proc. 2019; 94:2340–57. https://doi.org/10.1016/j.mayocp.2019.01.031 PMID:31054770

2. Tashiro N, Budhathoki S, Ohnaka K, Toyomura K, Kono S, Ueki T, Tanaka M, Kakeji Y, Maehara Y, Okamura T,

Ikejiri K, Futami K, Maekawa T, et al. Constipation and colorectal cancer risk: the Fukuoka colorectal cancer study. Asian Pac J Cancer Prev. 2011; 12:2025–30. PMID:22292645

3. Sumida K, Molnar MZ, Potukuchi PK, Thomas F, Lu JL, Yamagata K, Kalantar-Zadeh K, Kovesdy CP. Constipation and risk of death and cardiovascular events. Atherosclerosis. 2019; 281:114–20. https://doi.org/10.1016/j.atherosclerosis.2018.12.021 PMID:30658186

4. Coggrave M, Norton C, Cody JD. Management of faecal incontinence and constipation in adults with central neurological diseases. Cochrane Database Syst Rev. 2014; 1:CD002115. https://doi.org/10.1002/14651858.CD002115 PMID:24420006

5. Schiano di Visconte M, Pasquali A, Cipolat Mis T, Brusciano L, Docimo L, Bellio G. Sacral nerve stimulation in slow-transit constipation: effectiveness at 5-year follow-up. Int J Colorectal Dis. 2019; 34:1529–40. https://doi.org/10.1007/s00384-019-03351-w PMID:31309325

6. Black CJ, Ford AC. Chronic idiopathic constipation in adults: epidemiology, pathophysiology, diagnosis and clinical management. Med J Aust. 2018; 209:86–91. https://doi.org/10.5694/mja18.00241 PMID:29996755

7. Park C, Yan W, Ward SM, Hwang SJ, Wu Q, Hatton WJ, Park JK, Sanders KM, Ro S. MicroRNAs dynamically remodel gastrointestinal smooth muscle cells. PLoS One. 2011; 6:e18628. https://doi.org/10.1371/journal.pone.0018628 PMID:21533178

8. Suares NC, Ford AC. Prevalence of, and risk factors for, chronic idiopathic constipation in the community: systematic review and meta-analysis. Am J Gastroenterol. 2011; 106:1582–91. https://doi.org/10.1038/ajg.2011.164 PMID:21606976

9. Park C, Hennig GW, Sanders KM, Cho JH, Hatton WJ, Redelman D, Park JK, Ward SM, Miano JM, Yan W, Ro S. Serum response factor-dependent MicroRNAs regulate gastrointestinal smooth muscle cell phenotypes. Gastroenterology. 2011; 141:164–75. https://doi.org/10.1053/j.gastro.2011.03.058 PMID:21473868

10. Liu W, Zhang Q, Li S, Li L, Ding Z, Qian Q, Fan L, Jiang C. The relationship between colonic macrophages and MicroRNA-128 in the pathogenesis of slow transit constipation. Dig Dis Sci. 2015; 60:2304–15. https://doi.org/10.1007/s10620-015-3612-1 PMID:25749934

11. Viola MF, Boeckxstaens G. Intestinal resident macrophages: multitaskers of the gut. Neurogastroenterol Motil. 2020; 32:e13843. https://doi.org/10.1111/nmo.13843 PMID:32222060

12. Muller PA, Matheis F, Mucida D. Gut macrophages: key players in intestinal immunity and tissue physiology. Curr Opin Immunol. 2020; 62:54–61. https://doi.org/10.1016/j.coi.2019.11.011 PMID:31841704

13. Schemann M, Camilleri M. Functions and imaging of mast cell and neural axis of the gut. Gastroenterology. 2013; 144:698–704.e4. https://doi.org/10.1053/j.gastro.2013.01.040 PMID:23354018

14. Robinson AM, Rahman AA, Carbone SE, Randall-Demllo S, Filippone R, Bornstein JC, Eri R, Nurgali K. Alterations of colonic function in the Winnie mouse model of spontaneous chronic colitis. Am J Physiol Gastrointest Liver Physiol. 2017; 312:G85–G102. https://doi.org/10.1152/ajpgi.00210.2016 PMID:27881401

15. Liang C, Wang KY, Yu Z, Xu B. Development of a novel mouse constipation model. World J Gastroenterol. 2016; 22:2799–810. https://doi.org/10.3748/wjg.v22.i9.2799 PMID:26973418

16. Bao YG, Shu XL, Li XB, Gu WZ, Ying AJ, Zhao C, Ou BY, Jiang MZ. [Roles of enteric nervous system neurotransmitters and interstitial cells of Cajal in the colon in slow transit constipation in rats]. Zhongguo Dang Dai Er Ke Za Zhi. 2009; 11:481–85. PMID:19558815

17. Girón R, Pérez-García I, Abalo R. X-ray analysis of gastrointestinal motility in conscious mice. Effects of morphine and comparison with rats. Neurogastroenterol Motil. 2016; 28:74–84. https://doi.org/10.1111/nmo.12699 PMID:26486654

18. Velázquez Rivera I, Velázquez Clavarana L, García Velasco P, Melero Ramos C. Opioid-induced constipation in chronic pain: experience with 180 patients. J Opioid Manag. 2019; 15:69–76. https://doi.org/10.5055/jom.2019.0487 PMID:30855724

19. Farmer AD, Holt CB, Downes TJ, Ruggeri E, Del Vecchio S, De Giorgio R. Pathophysiology, diagnosis, and management of opioid-induced constipation. Lancet Gastroenterol Hepatol. 2018; 3:203–12. https://doi.org/10.1016/S2468-1253(18)30008-6 PMID:29870734

20. Liang X, Shangguan W, Zhang M, Mei S, Wang L, Yang R. miR-128 enhances dendritic cell-mediated anti-tumor immunity via targeting of p38. Mol Med Rep. 2017; 16:1307–13.

https://doi.org/10.3892/mmr.2017.6717
PMID:29067466

21. Liu J, Wang S, Zhang Q, Li X, Xu S. Selenomethionine alleviates LPS-induced chicken myocardial inflammation by regulating the miR-128-3p-p38 MAPK axis and oxidative stress. Metallomics. 2020; 12:54–64. https://doi.org/10.1039/c9mt00216b PMID:31720660

22. Pan J, Zhou C, Zhao X, He J, Tian H, Shen W, Han Y, Chen J, Fang S, Meng X, Jin X, Gong Z. A two-miRNA signature (miR-33a-5p and miR-128-3p) in whole blood as potential biomarker for early diagnosis of lung cancer. Sci Rep. 2018; 8:16699. https://doi.org/10.1038/s41598-018-35139-3 PMID:30420640

23. Li Y, Wang Y, Shen X, Han X. miR-128 functions as an OncomiR for the downregulation of HIC1 in breast cancer. Front Pharmacol. 2019; 10:1202. https://doi.org/10.3389/fphar.2019.01202 PMID:31680974

24. Ching AS, Ahmad-Annuar A. A perspective on the role of microRNA-128 regulation in mental and behavioral disorders. Front Cell Neurosci. 2015; 9:465. https://doi.org/10.3389/fncel.2015.00465 PMID:26696825

25. Cuadrado A, Nebreda AR. Mechanisms and functions of p38 MAPK signalling. Biochem J. 2010; 429:403–17. https://doi.org/10.1042/BJ20100323 PMID:20626350

26. Hume DA, MacDonald KP. Therapeutic applications of macrophage colony-stimulating factor-1 (CSF-1) and antagonists of CSF-1 receptor (CSF-1R) signaling. Blood. 2012; 119:1810–20. https://doi.org/10.1182/blood-2011-09-379214 PMID:22186992

27. Toh ML, Bonnefoy JY, Accart N, Cochin S, Pohle S, Haegel H, De Meyer M, Zemmour C, Preville X, Guillen C, Thioudellet C, Ancian P, Lux A, et al. Bone- and cartilage-protective effects of a monoclonal antibody against colony-stimulating factor 1 receptor in experimental arthritis. Arthritis Rheumatol. 2014; 66:2989–3000. https://doi.org/10.1002/art.38624 PMID:24623505

28. Han Y, Ma FY, Tesch GH, Manthey CL, Nikolic-Paterson DJ. C-fms blockade reverses glomerular macrophage infiltration and halts development of crescentic anti-GBM glomerulonephritis in the rat. Lab Invest. 2011; 91:978–91. https://doi.org/10.1038/labinvest.2011.61 PMID:21519331

29. Kubota Y, Takubo K, Shimizu T, Ohno H, Kishi K, Shibuya M, Saya H, Suda T. M-CSF inhibition selectively targets pathological angiogenesis and lymphangiogenesis. J Exp Med. 2009; 206:1089–102. https://doi.org/10.1084/jem.20081605 PMID:19398755

30. Menke J, Iwata Y, Rabacal WA, Basu R, Stanley ER, Kelley VR. Distinct roles of CSF-1 isoforms in lupus nephritis. J Am Soc Nephrol. 2011; 22:1821–33. https://doi.org/10.1681/ASN.2011010038 PMID:21885670

31. Menke J, Rabacal WA, Byrne KT, Iwata Y, Schwartz MM, Stanley ER, Schwarting A, Kelley VR. Circulating CSF-1 promotes monocyte and macrophage phenotypes that enhance lupus nephritis. J Am Soc Nephrol. 2009; 20:2581–92. https://doi.org/10.1681/ASN.2009050499 PMID:19926892

32 Muller PA, Koscsó B, Rajani GM, Stevanovic K, Berres ML, Hashimoto D, Mortha A, Leboeuf M, Li XM, Mucida D, Stanley ER, Dahan S, Margolis KG, Gershon MD, Merad M, Bogunovic M, et al. Crosstalk between Muscularis Macrophages and Enteric Neurons Regulates Gastrointestinal Motility. Cell. 2014; 158:1210. https://doi.org/10.1016/j.cell.2014.08.002 PMID:28917294

33. Zhang T, Yu J, Zhang Y, Li L, Chen Y, Li D, Liu F, Zhang CY, Gu H, Zen K. Salmonella enterica serovar enteritidis modulates intestinal epithelial miR-128 levels to decrease macrophage recruitment via macrophage colony-stimulating factor. J Infect Dis. 2014; 209:2000–11. https://doi.org/10.1093/infdis/jiu006 PMID:24415783

34. Hoi AY, Hickey MJ, Hall P, Yamana J, O'Sullivan KM, Santos LL, James WG, Kitching AR, Morand EF. Macrophage migration inhibitory factor deficiency attenuates macrophage recruitment, glomerulonephritis, and lethality in MRL/lpr mice. J Immunol. 2006; 177:5687–96. https://doi.org/10.4049/jimmunol.177.8.5687 PMID:17015758

35. Khan WI, Motomura Y, Wang H, El-Sharkawy RT, Verdu EF, Verma-Gandhu M, Rollins BJ, Collins SM. Critical role of MCP-1 in the pathogenesis of experimental colitis in the context of immune and enterochromaffin cells. Am J Physiol Gastrointest Liver Physiol. 2006; 291:G803–11. https://doi.org/10.1152/ajpgi.00069.2006 PMID:16728728

36. Cutolo M, Trombetta AC, Soldano S. Monocyte and macrophage phenotypes: a look beyond systemic sclerosis. Response to: 'M1/M2 polarisation state of M-CSF blood-derived macrophages in systemic sclerosis' by Lescoat et al. Ann Rheum Dis. 2019; 78:e128. https://doi.org/10.1136/annrheumdis-2018-214371 PMID:30269052

SUPPLEMENTARY MATERIALS

Supplementary Figures

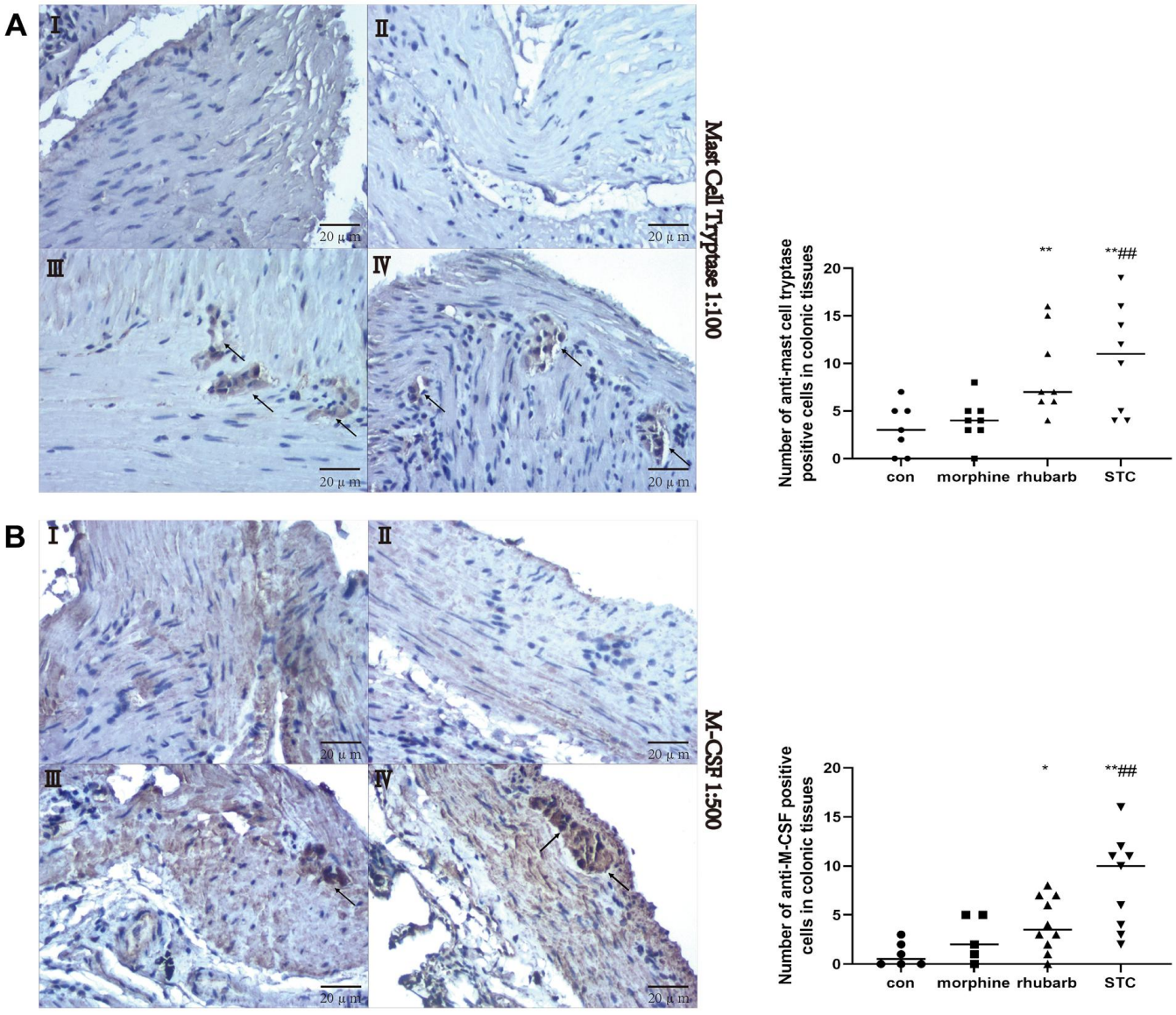

Supplementary Figure 1. The distribution of mast cell tryptase positive and M-CSF positive cells in colonic samples. (**A**) IHC staining (anti-mast cell tryptase) performed on colonic tissues [original magnification ×40]. I: saline group, II: morphine group, III rhubarb group, IV morphine+rhubarb group (STC) (**B**) IHC staining (anti-M-CSF) performed on colonic tissues [original magnification ×40]. I saline group, II: morphine group, III rhubarb group, IV morphine+rhubarb group (STC). *P <0.05 versus saline group, **P<0.01 versus saline group, #P<0.05 versus morphine group, ##P<0.01 versus morphine group.

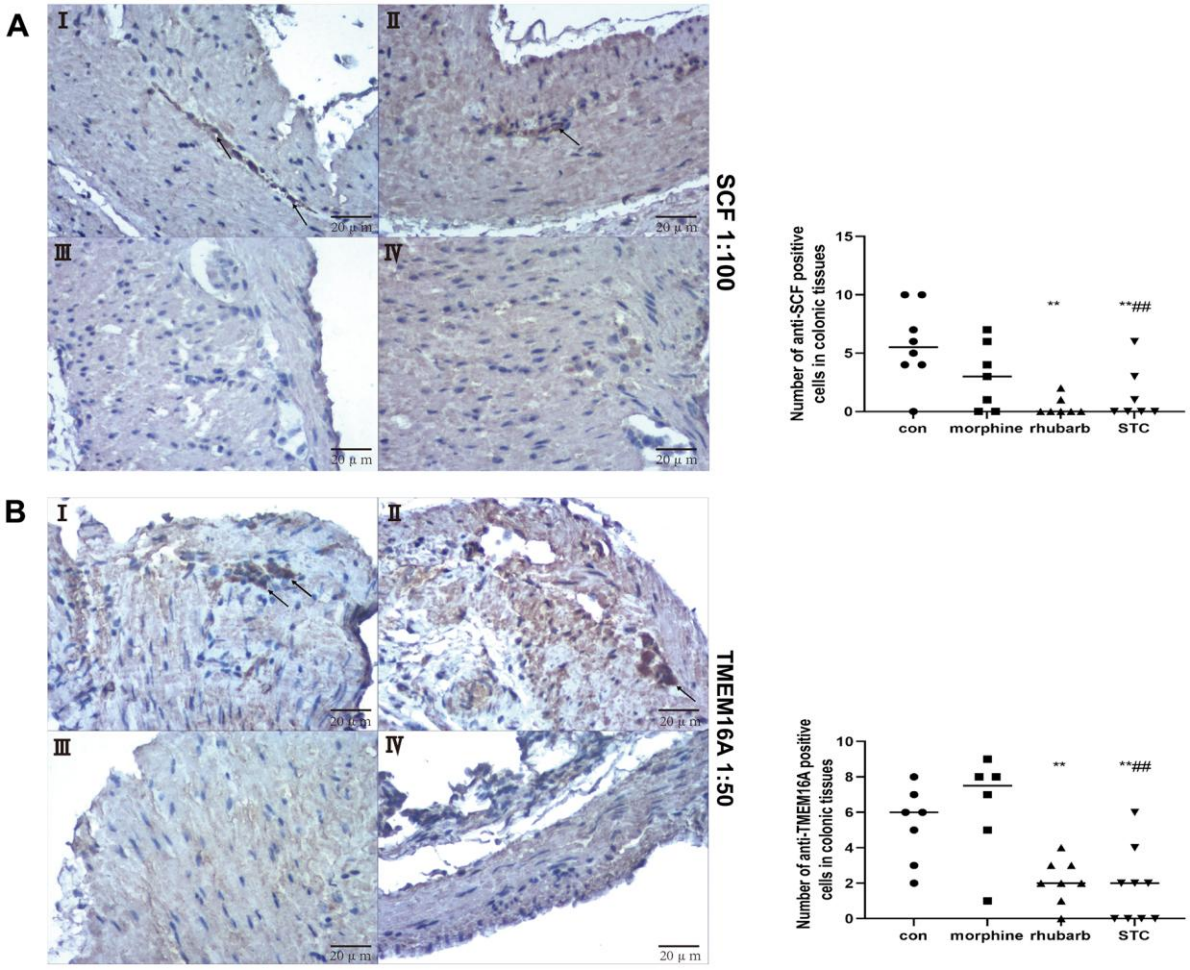

Supplementary Figure 2. The distribution of SCF positive and TMEM16A positive cells in colonic samples. (**A**) IHC staining (anti-SCF) performed on colonic tissues [original magnification ×40]. *I* saline group, *II:* morphine group, *III* rhubarb group, *IV* morphine+rhubarb group (STC) (**B**) IHC staining (anti-TMEM16A) performed on colonic tissues [original magnification ×40]. *I* saline group, *II:* morphine group, *III* rhubarb group, *IV* morphine+rhubarb group (STC). **P*<0.05 versus saline group, ***P*<0.01 versus saline group, #*P*<0.05 versus morphine group, ##*P*<0.05 versus morphine group.

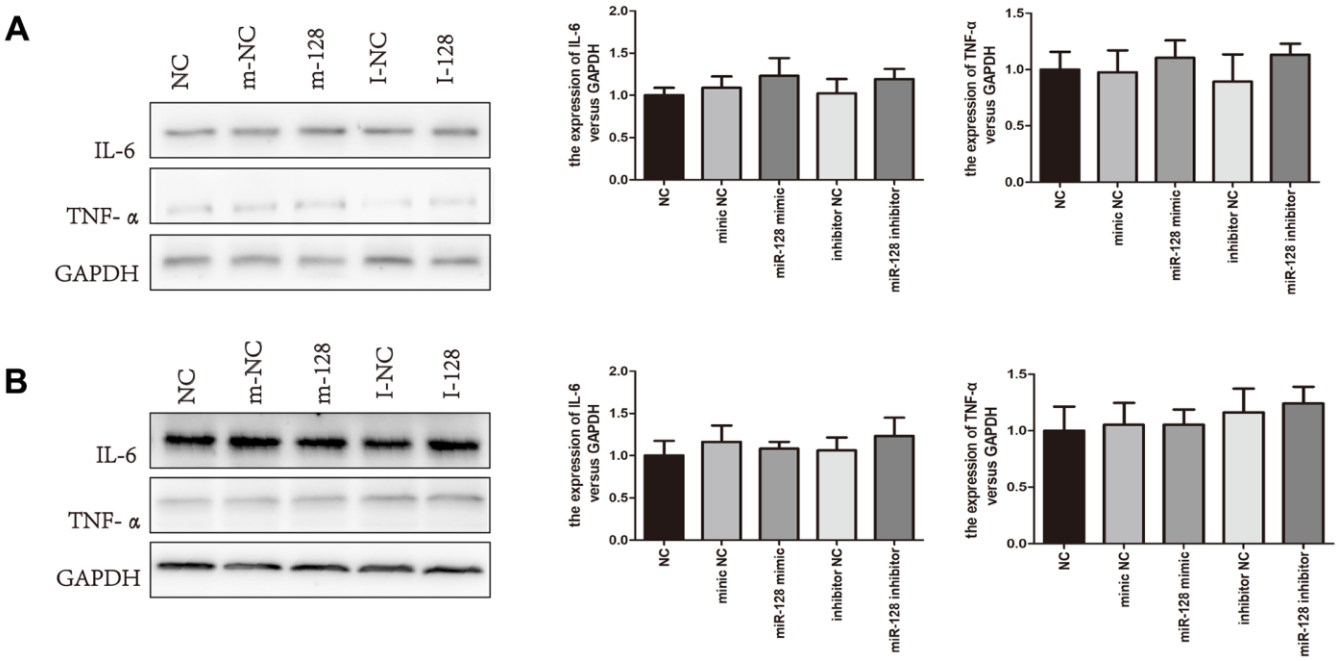

Supplementary Figure 3. The effect of microRNA-128 inhibitor on CT26.WT only or RAW264.7 only. (**A**) The protein expression levels of IL-6 and TNF-α after miR-128 interfered in CT26.WT cells. (**B**) The protein expression levels of IL-6 and TNF-α after miR-128 interfered in RAW264.7 cells.

Supplementary Tables

Supplementary Table 1. PCR primer.

U6		GTGCTCGCTTCGGCAGCACATATACTAAAATTGGAACGATACAGAGAAGATTA GCATGGCCCCTGCGCAAGGATGACACGCAAATTCGTGAAGCGTTCCATATTTT
mmu-miR-128-2		GGGGGCCGAUGCACUGUAAGAGA
mmu-miR-128-1		CGGGGCCGUAGCACUGUCUGA
GAPDH	F	TCCTGCACCACCAACTGCTTAG
	R	AGTGGCAGTGATGGCATGGACT
p38a-F	F	GCCCAGAAGGAGGCAGACT
	R	TGGGATGGCATGGAGTTGA
AKT	F	GGGTCCAGGGCCAAAGTC
	R	GAGAGGGCCAGTTAGCATACCA
M-CSF	F	TGCTGAGTCCCCCTTTCCT
	R	GACCACTCTCCTCCCAGATTCAT
Caspase-3	F	GCTCCTGGCCTCCTTATGG
	R	TGTGAGTTCCTTCCTTTCTTTGTG
Bax	F	CCCCCACATGGCAGACA
	R	CCTCAGCCCATCTTCTTCCA
Bcl-2	F	AGGCATGAAGAAAACCAGGTAGAG
	R	GGACTTGGTGCATGGAACACT
TNF-α	F	AGCACAAGGCTGAGATTCTCGC
	R	CTCGTTCAGTCTCCAGCTTCTG
IL-6	F	CGCTATGAAGTTCCTCTCTGCAA
	R	TAGGGAAGGCCGTGGTTGT
IL-8	F	TACTAGCCTGCATCAGCATGG
	R	TGGCTATGCACACAAACTTGAC
IL-10	F	GTTGCCAAGCCTTATCGGAA
	R	TGATTTCTGGGCCATGCTTCT
TGF-β	F	GGACTCTCCACCTGCAAGAC
	R	CTGGCGAGCCTTAGTTTGGA
SCF	F	ACTCTGTCTTGAGGCTGCATGTAA
	R	AAAGAAGAGCAGCCACCATGTAC
NSE	F	CTGCCCTGACCTGCCATAGT
	R	GAACAGCAGGAGCGGTGAGT

Supplementary Table 2. Antibody information.

Gene	Company	Cat No.	Dilution	Secondary antibody
GAPDH	Abcam	ab181603	1:5000	Anti-rabbit from goat
M-CSF	Abcam	ab233387	1:5000	Anti-rabbit from goat
SCF	Proteintech	26582-1-AP	1:1000	Anti-rabbit from goat
NSE	Proteintech	10149-1-AP	1:1000	Anti-rabbit from goat
p38 MAPK	Proteintech	14064-1-AP	1:1000	Anti-rabbit from goat
IL-6	Proteintech	21865-1-AP	1:1000	Anti-rabbit from goat
TNF-α	Proteintech	17590-1-AP	1:1000	Anti-rabbit from goat